Research Paper

Micromotion and friction evaluation of a novel surface architecture for improved primary fixation of cementless orthopaedic implants

N. Harrison[a], P.E. McHugh[a], W. Curtin[b], P. Mc Donnell[a],*

[a]Mechanical and Biomedical Engineering, National University of Ireland, Galway, Ireland
[b]Merlin Park Hospital, Galway, Ireland

ARTICLE INFO

ABSTRACT

A new surface architecture (OsteoAnchor) for orthopaedic stem components has been developed, which incorporates a multitude of tiny anchor features for embedding into the bone during implantation. It was tested for its ability to provide improved primary fixation compared to existing surface coatings. Friction testing was performed on bovine trabecular bone. It was found that OsteoAnchor provided up to 76% greater resistance to transverse motion under simultaneous normal loading compared to the porous tantalum. Micromotion testing was performed on stem components implanted in cadaver ovine femurs. The micromotion amplitudes for the OsteoAnchor stem were significantly lower than for a corresponding plasma sprayed stem. These results demonstrate that OsteoAnchor has the potential to provide improved primary fixation for stem components in joint replacement operations.

1. Introduction

Effective long-term fixation of cementless orthopaedic stem implants is achieved by in-growth of hard bone tissue from the patient's own bone into the porous surface coating on the implant (Valle et al., 2004). Two processes are required for this to occur. Primary (initial) fixation is obtained by a press-fit approach during surgery, where the stem is forced into an undersized, reamed cavity. Secondary (long term) fixation is obtained via bone in-growth, where the bone tissue grows into surface pores on the stem. Effective primary fixation is critical to achieving secondary fixation (Chang et al., 2011; Chanlalit et al., 2011; Gebert et al., 2009; Gotze, et al., 2002; Sakai et al., 2006). If the implant exhibits excessive micromotions relative to the bone, fibrous bone tissue grows into the surface coating instead of hard bone (Cook et al., 1991; Soballe et al., 1992; Viceconti et al., 2001), resulting in inadequate fixation of the implant. Experimental studies have shown that micromotion levels below 40–70 µm are conducive to hard bone in-growth, while micromotions in excess of 150 µm result in fibrous tissue in-growth (Bragdon et al., 1996; Engh et al., 1992; Pilliar et al., 1986). Revision surgery may ultimately be required due to loosening of the stem if insufficient hard bone in-growth is not achieved, and this problem is particularly relevant for patients with poor bone quality (Dayton and Incavo, 2005; Krischak et al., 2003).

There are many surface coatings available for cementless orthopaedic implants, all of which rely on press-fit and friction

*Corresponding author. Tel.: +353 91 492 963.
E-mail addresses: noelharrisonnuig@gmail.com (N. Harrison), peter.mchugh@nuigalway.ie (P.E. McHugh), patmcd22@gmail.com (P. Mc Donnell).

between the coating and the patient's bone to achieve primary fixation. Well established coatings include sintered bead, plasma sprayed, wire mesh and hydroxyapatite. More recently, highly porous metal coatings have been evaluated for cementless orthopaedic implants (Benazzo et al., 2010; Bertollo et al., 2011; Bobyn et al., 1999; Frenkel et al., 2004; Meneghini et al., 2010). As well as their higher porosity compared to sintered bead or plasma sprayed coatings, these newer coatings have a higher reported coefficient of friction when tested on bone (Bourne et al., 2008; Gilmour et al., 2009; Levine and Fabi, 2010; Shirazi-Adl et al., 1993; Zhang et al., 1999) and this is considered to be an advantage in providing improved primary fixation for orthopaedic implants.

In vitro experimental approaches for evaluating the potential of a coating to provide good primary fixation in stem components have involved two approaches: (1) testing of the coating for coefficient of friction against a bone substrate; (2) performance of physiological cyclic loading of the stem implanted in either a synthetic or cadaver femur, with direct measurement of the resulting micromotions. A number of methods have been employed to perform friction coefficient testing, including the inclined plane technique (Zhang et al., 1999) and custom techniques where controlled loading is applied in the normal direction while the resistance to motion is simultaneously measured in the tangential direction (Biemond et al., 2011; Shirazi-Adl et al., 1993). Direct micromotion measurement tests for implanted stems have generally involved cyclic loading of the stem in a uniaxial testing machine and using LVDTs to detect the magnitude of the micromotions (Britton et al., 2004; Gortz et al., 2002; Kassi et al., 2005). Both synthetic femurs (Park et al., 2010; Race et al., 2011) and cadaver femurs (Ostbyhaug et al., 2010; Westphal et al., 2006) have been used for these tests.

The objective of this study was to evaluate the friction and micromotion characteristics of a new surface architecture (OsteoAnchor) that has been developed for cementless orthopaedic stem components at the authors' laboratory. The surface architecture is specifically designed to reduce micromotions of the stem after implantation by incorporating a multitude of small anchor features which are built onto a porous lattice substructure (Fig. 1). The anchor features embed into the patient's bone during implantation and help to provide immediate mechanical fixation of the implant. The Direct Metal Laser Sintering (DMLS) process is used to manufacture the implant core, porous surface architecture and anchor features as a single component. Friction testing was performed on small scale coupons of the OsteoAnchor surface architecture and other surface coatings that are commercially available. Micromotion testing was performed on large scale stem components incorporating the surface architecture which were implanted in cadaver ovine femurs. This test work was performed to test the hypothesis that the anchor features of the Osteoanchor surface architecture would provide better friction properties and micromotion resistance compared to currently available surface coatings such as plasma sprayed and porous tantalum.

2. Materials and methods

Custom test methods were developed to evaluate the friction performance of the OsteoAnchor surface architecture and
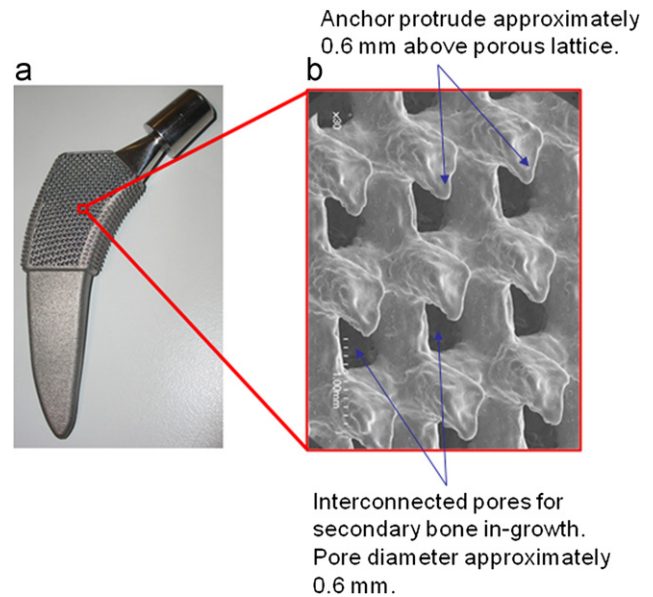

Fig. 1 – OsteoAnchor surface architecture, showing: (a) a hip stem implant incorporating the surface architecture; (b) a SEM magnified image of the surface architecture.

its resistance to micromotions under physiological loading conditions.

2.1. Friction testing

Three different surface architectures were tested for friction properties: OsteoAnchor, porous tantalum and plasma sprayed titanium. Circular coupons of each surface architecture were manufactured for testing. The porous tantalum coupon was cut from a commercially available hip stem component using the wire erosion cutting technique. The porosity of this surface coating was approximately 70%. The plasma sprayed coupon was manufactured using a DMLS produced, bare titanium coupon which was plasma sprayed with a 0.5 mm thick coating of commercially pure titanium with a porosity of at least 30% (Orchid Orthopaedic Solutions, MI, USA). The OsteoAnchor coupon was manufactured in one step using the DMLS process (3TRPD, Berkshire, UK) and incorporated a porosity of approximately 63%. All coupons were 15 mm diameter (Fig. 2).

A custom testing apparatus was developed to perform the testing, consisting of a loading arm which was mounted on the actuator of a combined axial-torsion Instron testing machine (Model 8874, Instron UK Ltd.). The test coupon of the surface architecture was fixed onto the end of the loading arm and brought into contact with a milled flat block of bovine trabecular bone which had been clamped securely onto the frame of the Instron testing machine (Fig. 3). A nominal normal load was applied between the test coupon and the bone by adjusting the axial position of the loading arm. Transverse motion was then applied via the torsional actuator which moved the test coupon in a wide arc on the bone sample via the loading arm radius. For each test, a torsional motion of 1° was applied at a rate of 1°/s. The axial load, axial position, torque and angular position were recorded continuously during the test. The instantaneous
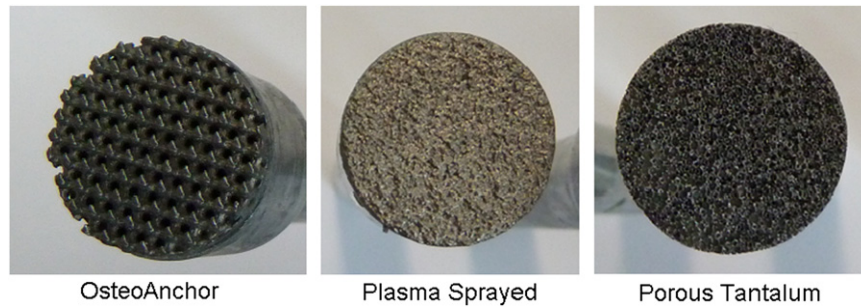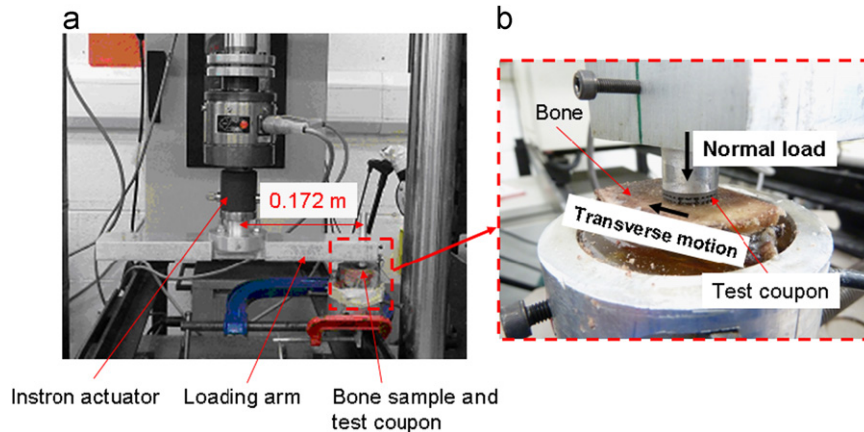
Fig. 2 – Coupons for friction testing.

Fig. 3 – Test setup for friction performance evaluation showing: (a) overall test setup in Instron testing machine; (b) close up view of test coupon on bone.

transverse reaction load was calculated by dividing the recorded torque value by the length of the moment arm of the loading arm (0.172 m). The ratio of the transverse load to the normal load (T/N ratio) was calculated from the recorded data to give a measure of the friction coefficient between the test coupon and the bone sample. The first peak value of T/N ratio and the maximum peak value of T/N ratio for the duration of the test were noted. Tests were performed at two levels of applied normal load to determine its effect on the resulting T/N ratio: 100 N and 150 N. Five test repetitions were performed for each test coupon at each normal load value. When a series of tests were complete, the bovine bone sample was milled by 0.2 mm to ensure that a fresh layer of trabecular bone was presented to the test coupon for subsequent tests.

2.2. Micromotion testing

A custom designed stem for ovine femurs was used for the micromotion study. This stem geometry had been previously developed for a pre-clinical trial of the OsteoAnchor technology (Fig. 4). One stem incorporated the OsteoAnchor surface architecture and was manufactured using DMLS technology (3TRPD, Berkshire UK). The other stem incorporated a standard plasma-sprayed CP titanium surface coating of thickness 0.5 mm and porosity of approximately 30%. The core of this stem had the same geometry as the OsteoAnchor stem and the coating was plasma sprayed onto this core by
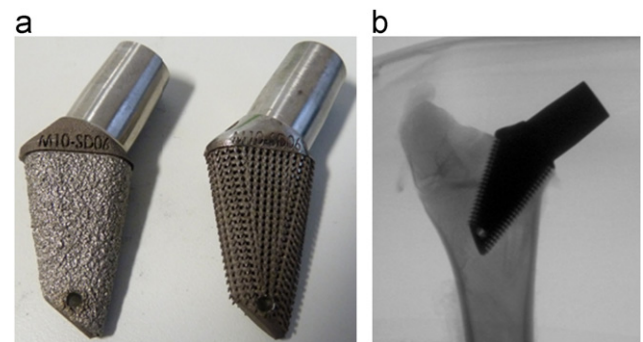

Fig. 4 – Implants for primary fixation test showing: (a) custom designed ovine hip implants with plasma sprayed surface (left) OsteoAnchor surface (right); (b) X-ray picture of the stem implanted in an ovine femur to give a press fit.

a commercial orthopaedics company (Orchid Orthopaedic Solutions, MI, USA). The stems were implanted into ovine femurs which were obtained from an abbatoir, using a custom-made set of instrumentation and broaches. This resulted in a press-fit between the stem and the trabecular bone in the metaphysis of the femur (Fig. 4).

Two locations on the stem were monitored for micromotions: the exposed proximal portion of the implant (i.e. the shoulder and neck region) and the distal end of the implant. A video extensometer (VE) was used to track the relative micro-movement of the bone and implant at these locations via parallel tracking markers on the bone and the implant
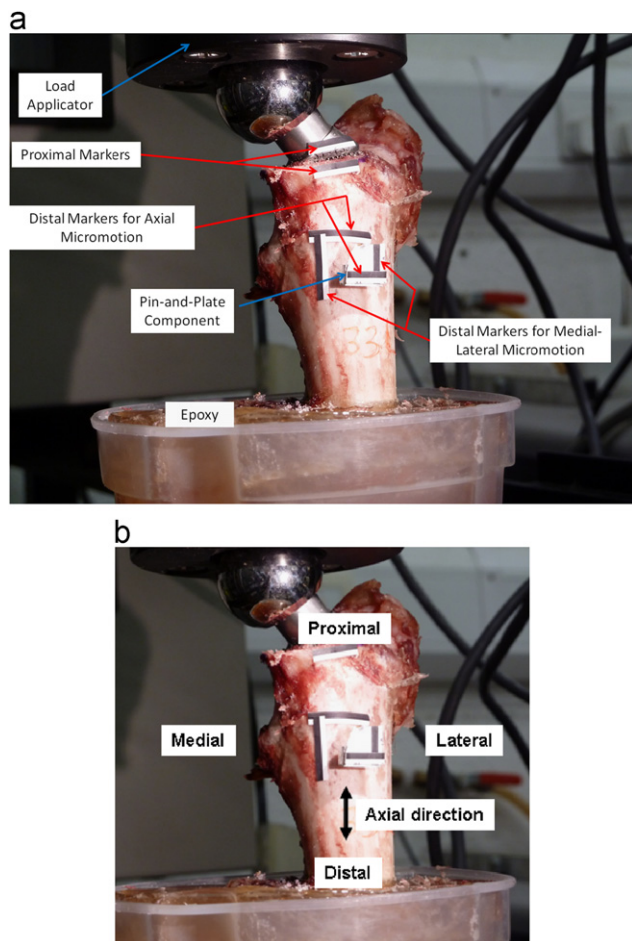
Fig. 5 – Micromotion test setup showing: (a) components of test set-up; (b) definition of direction protocol for identifying motions.

Table 1 – Recording profile for the friction test load cycles.	
Cycle number	**Region**
0–300	Proximal (axial)
300–600	Distal (axial and M–L)
600–5000	No VE recording
5000–300	Proximal (axial)
5300–5600	Distal (axial and M–L)
5600–10,000	No VE recording
10,000–10,300	Proximal (axial)
10,300–10,600	Distal (axial and M–L)

the stem. A 22 mm diameter Co–Cr femoral head component was fitted onto the standard 12/14 Morse taper neck of the stem. Loading was applied to the femoral head by a concave load applicator which was attached to the actuator of the Instron. Loading was applied for 10,600 cycles and ranged from 20 N to 220 N, providing a peak load which was approximately 40% of a sheep's body weight (taken to be 55 kg). A sinusoidal wave pattern was used at a frequency of 3 Hz.

The video extensometer could analyse only one region at a given time. Therefore, a recording profile as detailed in Table 1 was used for recording the micromotion data. Subsidence of the stem was not measured due to the fact that the VE could not be used to continuously record the axial displacement at one location for the complete duration of the test. In total, five femurs were implanted and tested with OsteoAnchor stems and a further five femurs were implanted and tested with plasma sprayed stems.

(Fig. 5). The repeatability and accuracy of the VE was initially tested to ensure that it would be sufficiently sensitive to measure the small micromotions that would be obtained for the implanted stems.

In order to track the micromotions at the distal end of the stem (which is fully enclosed by the femur), a pin and plate component was inserted through a 5 mm diameter hole that was drilled at the appropriate location on the femur and the pin was push-fit into a corresponding hole in the stem (Fig. 5). The plate part of the component allowed the markers for the VE to be attached and corresponding parallel markers were attached to the external bone of the femur. At the proximal end of the stem, the arrangement of the tracking markers allowed recording of the micromotion in the axial direction only. At the distal end, the arrangement of the tracking markers allowed recording of the micromotion in both the axial and medial–lateral (M–L) directions.

Each femur with the implanted stem was potted in epoxy resin so that the distance between the surface of the epoxy and the centre point of the implant/osteotomy junction was consistently 110 mm. A positioning fixture was used to achieve an angle of adduction of 10° and an angle of flexion of 9°, relative to the axis of the femur to generate a combination of axial, bending and torsional loading on

3. Results

3.1. Friction testing

A typical plot of the transverse to normal force (T/N) ratio versus time for the OsteoAnchor test coupon (Fig. 6) shows that there is a linear increase to an initial peak value followed by a non-linear region where a second, maximum peak value occurs. No sliding of the coupon occurs up to the first peak value. The maximum peak occurs in the non-linear region and is caused by the local features of the surface architecture interacting with the pore walls of the trabecular bone structure as the coupon moves over the bone, thus giving rise to greater transverse resistance.

OsteoAnchor exhibited a higher T/N ratio than either porous tantalum or plasma sprayed at both the first peak value and the maximum peak value (Fig. 7 and Table 2). This was the case for both the 100 N normal load and the 150 N normal load. This higher T/N ratio was statistically significant for all cases except for the OsteoAnchor-porous tantalum comparison at first peak load, 100 N normal load (comparisons made using Student T-test at 95% confidence level). The increase in T/N ratio for OsteoAnchor was greater for the 150 N normal load compared to the 100 N normal load, and particularly so for the maximum peak T/N ratio at 150 N. In this case, the OsteoAnchor T/N ratio of 2.84 was 74% greater than that for the porous tantalum coupon (1.63) and 246% greater than that for the plasma sprayed coupon (0.82).
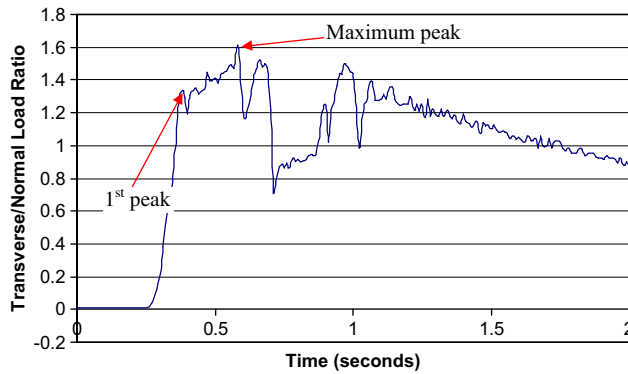
Fig. 6 – Typical transverse/normal load ratio vs time for a single test, OsteoAnchor coupon at 100 N nominal normal load.
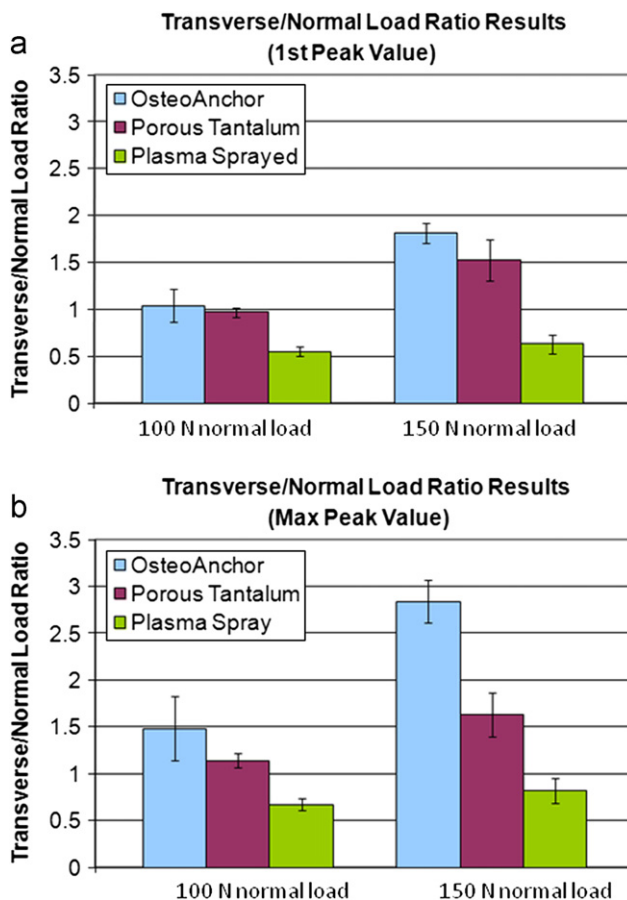

Fig. 7 – (a) T/N ratio at first peak value. (b) T/N ratio at maximum peak value.

It was found that the normal load between the test coupon and the bone did not remain constant, despite the fact that the test was carried out in load control. A drop off in normal load occurred once the transverse motion was applied (Fig. 8). Although the Instron actuator compensated for this load drop-off by moving the token in an axial direction towards the bone, the controller was not responsive enough to achieve this until the transverse motion of the token had ceased. It was found that the actual normal loads at the first and maximum peak values were lowest for the OsteoAnchor

coupon. Although this contributed to the high T/N ratios for the OsteoAnchor coupon, it can be seen from Table 2 and Fig. 9 that even for lower normal loads, the resulting transverse resisting loads were higher for OsteoAnchor. Again, this was particularly the case for the 150 N normal load.

Qualitatively, the embedding of the OsteoAnchor anchor features could be clearly seen at the 150 N normal load. This was evident by the characteristic tracks left in the trabecular bone sample (Fig. 10). In addition, particles of bone and marrow could be seen to be lodged between the claw features of the OsteoAnchor test coupon (Fig. 10). This type of interaction with the trabecular bone was not seen with either the porous tantalum or the plasma sprayed test coupons.

3.2. Micromotion testing

The repeatability of the VE for measuring micromotion amplitudes was found to be within 2.0 µm over a displacement range of 0–100 µm. The accuracy was found to be within 3 µm over the same measurement range.
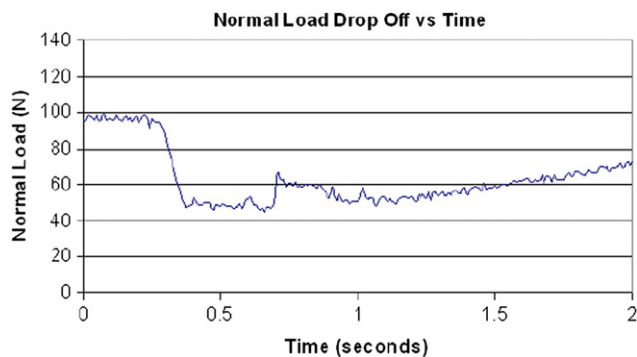
The magnitude of micromotions was determined by calculating a moving average of the cyclic displacement amplitude. The deviation of each displacement data point from the moving average value at a given time point was determined and was used to calculate an effective standard deviation. This standard deviation was then doubled, to give the range of data encompassing 95% of the data points, assuming a normal distribution around the moving average. As seen in a typical displacement versus time plot (Fig. 11), this provides a good measure of the amplitude of micromotions of the test specimen. All statistical comparisons between the OsteoAnchor and plasma spray results were carried out using the Student T-test.

The average micromotion results for each data sample indicated that the OsteoAnchor stem had a consistently lower magnitude of mean micromotion compared to the plasma sprayed stem (Table 3 and Fig. 12). The mean OsteoAnchor micromotion was significantly lower than that of the plasma spray stem for motion in the axial direction at the proximal location ($p < =0.015$) and for motion in the medial–lateral direction at the distal end ($p < =0.005$). However, there was no statistical difference in axial motion at the distal end between the two test groups. Grouping the micromotion results of all measurements taken (Fig. 13) indicated a significantly lower mean value of micromotion for the OsteoAnchor stem compared to the plasma spray stem ($p < =0.001$).

The micromotion amplitudes increased for both the OsteoAnchor and plasma spray stems as the number of cycles of testing progressed (Fig. 14). However, the relative increase in micromotion amplitude was greater for the plasma spray stem. From the start of the test to the 5000 cycle stage, there was an increase in the mean value of the micromotion averaged for all locations on the stem, of 15.3% for the plasma spray stem compared to 4.0% for the OsteoAnchor stem. Similarly, from the start of the test to the 10,000 cycle stage, the increase in micromotion amplitude was 33.9% for the plasma spray stem compared to 22.0% for the OsteoAnchor stem.

Table 2 – Results of friction tests for OsteoAnchor, porous tantalum and plasma spray surface architectures.

Test result	OsteoAnchor (mean± std. dev.)	Porous tantalum (mean± std. dev.)	Plasma spray (mean± std. dev.)
100 N applied normal load			
First peak T/N ratio	1.04±0.18	0.97±0.05	0.55±0.05
Max peak T/N ratio	1.48±0.34	1.14±0.08	0.67±0.06
Transverse load at first peak (N)	56.3±11.3	53.3±5.4	37.5±2.4
Transverse load at max peak (N)	66.1±11.1	57.7±6.4	42.0±4.4
Normal load at first peak (N)	54.4±11.4	55.1±5.6	69.0±5.8
Normal load at max. peak (N)	45.8±9.7	50.4±5.5	62.6±4.3
150 N applied normal load			
First peak T/N ratio	1.81±0.11	1.52±0.22	0.63±0.1
Max peak T/N ratio	2.84±0.23	1.63±0.23	0.82±0.13
Transverse load at first peak (N)	116.7±9.1	108.3±16.4	64.2±10.4
Transverse load at max peak (N)	156.8±14.3	109.5±18.8	79.4±17.0
Normal load at first peak (N)	64.7±5.5	71.1±7.7	101.6±9.6
Normal load at max. peak (N)	56.0±6.3	67.3±2.8	96.7±9.3

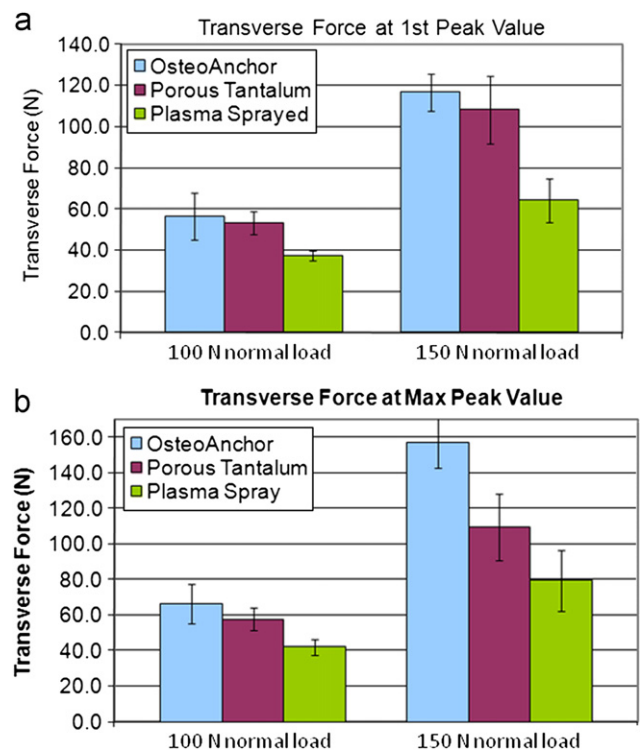Fig. 8 – Normal load drop off vs time, porous tantalum coupon under 100 N normal load.

For both the OsteoAnchor and plasma sprayed stems, the highest micromotions occurred at the distal location. This was expected since rotation-type motions that initiate at the proximal end of the stem are amplified distally by the lever-arm effect of the stem length. The maximum micromotion amplitude for the OsteoAnchor stem, averaged for the five femurs tested, was 10.48±7.39 μm and this occurred in the axial direction at the distal location of the stem. For the plasma sprayed stem, the maximum micromotion amplitude was 16.14 μm and also occurred at the distal location, but in the M–L direction.

Fig. 9 – Transverse force values at (a) first peak value and (b) maximum peak value.

4. Discussion

The results of this study have demonstrated the potential of the newly developed OsteoAnchor surface architecture to provide improved primary fixation of cementless stem components in orthopaedic joint replacement applications. For both the small scale coupon friction testing and large scale stem micromotion testing, OsteoAnchor performed better than commercially available surface coatings.

The friction testing examined the ability of the surface architecture to resist transverse motion across a trabecular bone surface while normal loading was simultaneously being applied to provide a pressure force between the surface architecture and the bone. The ratio of the resisting transverse force divided by the applied normal force (T/N ratio) was determined for coupons of OsteoAnchor, porous tantalum and plasma sprayed surface architectures at applied normal loads of 100 N and 150 N. The custom test method that was developed gave T/N results which corresponded well with those reported in the literature. For example, the first peak T/N ratio for the porous tantalum was found to be 0.97 compared to 0.98 as reported in a study which employed the
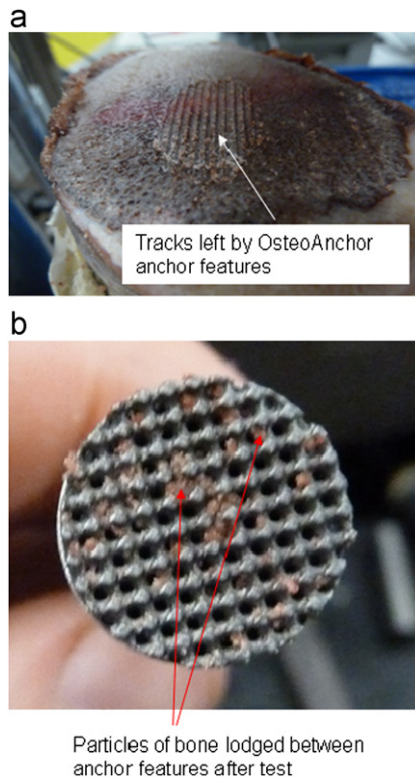
Fig. 10 – Photographs showing how OsteoAnchor anchor features embed into the bone: (a) bone sample with characteristic OsteoAnchor embedding tracks after test is completed; (b) OsteoAnchor test coupon after test with particles of bone lodged in between claws.
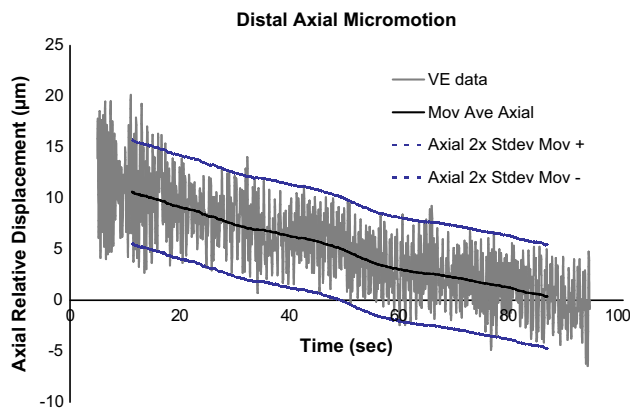

Fig. 11 – Typical relative displacement plot: distal portion of OsteoAnchor, 300–600 cycles. Blue lines represent the moving average of the micromotion amplitude. (For interpretation of the references to colour in this figure caption, the reader is referred to the web version of this article.)

peak T/N ratio increased to 74% greater than porous tantalum and 246% greater than plasma sprayed.

For stem applications in orthopaedic joint replacement, the T/N ratio provides a measure of the resistance of the stem to motion in the direction of the applied physiological loads (transverse direction), while simultaneously being press-fit against the internal bone of the prepared cavity for the stem (normal direction). OsteoAnchor performed better than either porous tantalum or plasma sprayed surfaces in this regard, and this performance improved as the applied normal load was increased from 100 N to 150 N. This was due to the fact that the embedding action of the OsteoAnchor claws was more effective under the higher normal load of 150 N. Visually, the embedding could be clearly seen for the 150 N normal load as a series of parallel tracks left in the trabecular bone surface (Fig. 10).
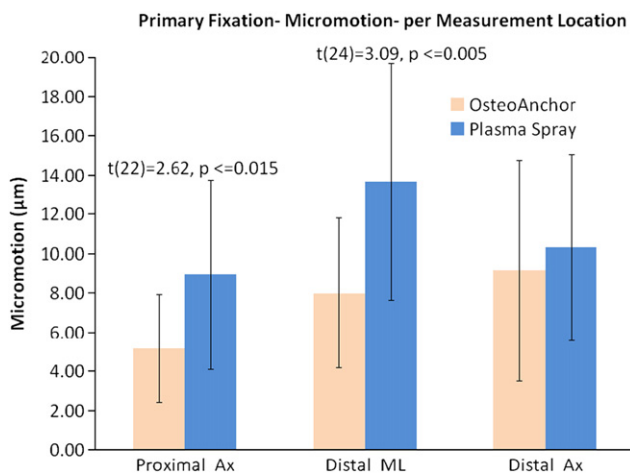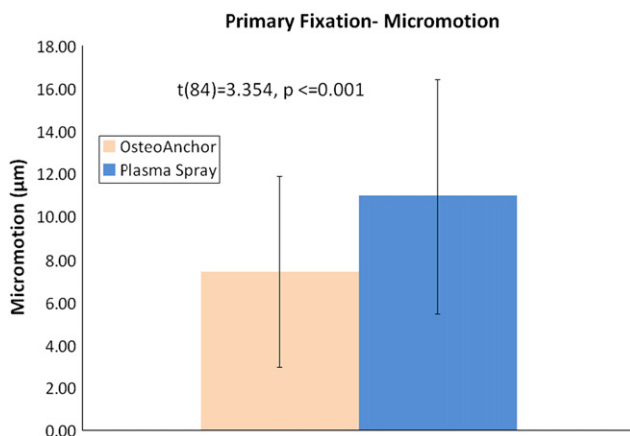
The 150 N normal load corresponds to an applied pressure of 0.85 MPa between the 15 mm diameter token and the bone surface. Although this normal pressure is higher than that used for other friction testing studies, e.g. 0.17 MPa applied by Biemond et al. (2011), it is an order of magnitude lower than the normal pressure which would be generated during implantation of a hip stem in vivo. Finite element analysis studies have shown that an interference fit of 100 μm during implantation between the stem and the internal bone of the prepared cavity results in a hoop stress in the order 50 MPa (Abdul-Kadir, et al., 2008). If the shaft of the femur is approximated as a thick walled cylinder of internal diameter 20 mm and external diameter 30 mm, the internal pressure required to generate a circumferential stress of this magnitude would be in the order of 20 MPa. This would equate to the pressure that is generated between the surface of the stem and the internal cavity of the bone when the surgeon press-fits the stem into place in the femur. The 0.85 MPa pressure that is generated in the current testing between the surface architecture token is considerably lower than this in vivo value. It was not possible to increase this normal pressure beyond 0.85 MPa because the resultant transverse loads that were generated exceeded the load cell capacity of the test machine.

For the large scale testing, cyclic loading of a stem component in an ovine femur was carried out and the resulting micromotions were measured using a video extensometer. The stem design was conservative in geometry (short stem design) and engagement of the stem surface with the host bone occurred only in the metaphyseal region of the femur. Such a conservative design is being increasingly employed for hip joint replacement operations in order to preserve as much bone stock as possible for potential future revision operations (Kluge, 2009). The hip stem design for this study was, therefore, considered relevant for current orthopaedic hip stem applications.

Testing was performed on two stems with identical geometries, one with an OsteoAnchor surface architecture and one with a plasma sprayed surface architecture. The micromotion values that were obtained for the OsteoAnchor stem were consistently lower than for the plasma sprayed stem. The highest mean micromotion value for OsteoAnchor was 10.48 μm compared to 16.14 μm for the plasma sprayed stem. In addition, the increase in micromotion levels as the number of test cycles progressed was much lower for OsteoAnchor compared to the plasma sprayed stem, suggesting that OsteoAnchor

inclined plane method (Zhang et al., 1999). Similarly, for the plasma sprayed token, the first peak T/N ratio was found to be 0.55 compared to 0.64 as reported by Biemond et al. (2011). It was found that the mean peak T/N ratio for OsteoAnchor at the 100 N normal load was 30% greater than that for porous tantalum and 121% greater than that for plasma sprayed. For the 150 N normal load, the improvement in the OsteoAnchor
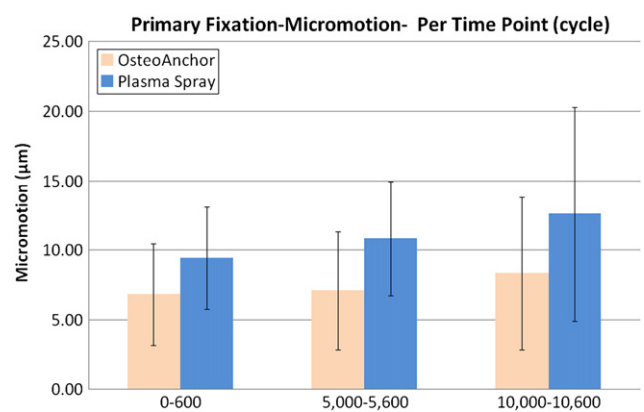
Table 3 – Mean and standard deviation of micromotion amplitude of OsteoAnchor and Plasma Spray stems ($n = 5$ for both groups).

Location	Cycle	OsteoAnchor (μm)	Plasma spray (μm)
Proximal Ax 1	0–300	4.85 ± 1.84	6.62 ± 1.50
Distal ML 1	300–600	7.16 ± 3.38	12.37 ± 2.34
Distal Ax 1	300–600	8.46 ± 4.79	9.24 ± 4.30
Proximal Ax 2	5000–5300	4.69 ± 2.19	10.50 ± 4.70
Distal ML 2	5300–5600	8.16 ± 4.22	12.44 ± 1.84
Distal Ax 2	5300–5600	8.43 ± 5.40	9.60 ± 5.27
Proximal Ax 3	10,000–10,300	5.92 ± 4.19	9.63 ± 6.81
Distal ML 3	10,300–10,600	8.58 ± 4.47	16.14 ± 10.33
Distal Ax 3	10,300–10,600	10.48 ± 7.39	12.02 ± 5.13

Fig. 12 – Micromotion mean and standard deviation results for each measurement location, averaged over all recorded test cycles.

Fig. 13 – Mean and standard deviation micromotion magnitude of all micromotion measurements.

Fig. 14 – Mean and standard deviation micromotion results, averaged for all locations, at each test cycle recording period.

is a more stable implant for long-term operation. These results demonstrate the ability of the OsteoAnchor surface architecture to provide better primary fixation than conventional plasma spray surface coatings in a realistic physiological test setup.

The results of the current study are not directly comparable with other micromotion studies on human femurs since the bone type, stem geometry and loading conditions are different. In general, the micromotion levels reported for human femur studies are higher (in the region of 100–500 μm) than those obtained in the current study due to the fact that higher cyclic loading levels (in the region of 1000–2000 N) are applied (Monti, et al., 1999; Nogler, et al., 2004; Westphal et al., 2006). However, the high variability in the micromotion levels between different tests that were observed for this study (Table 3 and Figs. 12 and 13) has also been reported in studies for human femurs (Maher, et al., 2001; Park et al., 2010; Race et al., 2011). This high variability is due to a variety of factors including variability in the geometry and bone quality of the femurs used and variability in the implantation of the stem in the femur.

Limitations in the current study include the fact that it was not possible to maintain a constant normal load for the friction tests due to the inability of the test machine controller to adjust for the normal load drop off which occurred as the test progressed (Fig. 8). However, since the transverse resistance load will decrease as the applied normal load decreases, the value of the reported T/N ratio should not be affected. In addition, even though the normal load drop off was found to be greatest for the OsteoAnchor coupon, the corresponding transverse resistance load was still greater than that for the porous tantalum or plasma sprayed coupons (Table 2 and Fig. 9). Therefore, the normal load drop off that

occurred does not affect the conclusion that the OsteoAnchor surface architecture provides better resistance to transverse motion than the other surface coatings that were tested.

For the large scale micromotion tests, it was unfeasible to coat the custom-made stems with porous tantalum, and therefore, the comparison was limited to OsteoAnchor and a stem with a standard plasma sprayed coating. A limitation of this part of the study was that a relatively small number of specimens were tested, i.e. five femurs were tested for each stem type. Despite this small number of specimens, the micromotion results indicated that the OsteoAnchor surface architecture provided better resistance to micro-motion compared to the plasma sprayed surface coating, and this improvement was statistically significant. A further limitation of the micromotion tests was that the subsidence of the stems could not be measured. This was not possible due to the discontinuities in the recording profile that were required with the video extensometer in order to monitor the different locations on the stem (Table 1). Future work will focus on continuous recording of the stem motion at a single location for the complete duration of the test so that the subsidence performance of the OsteoAnchor surface archi-tecture can be determined.

5. Conclusions

The results of the small scale friction tests and large scale micromotion tests have shown that the OsteoAnchor sur-face architecture has the potential to provide significantly improved primary fixation for stem components in joint replacement applications compared to existing surface coatings that are available. This will help to ensure that hard bone, rather than fibrous tissue, grows into the porous substructure under the anchor features, providing long-term, secure fixation of the implant.

REFERENCES

Abdul-Kadir, M.R., et al., 2008. Finite element modelling of primary hip stem stability: the effect of interference fit. Journal of Biomechanics 41, 587–594.

Benazzo, F., et al., 2010. Our experience with the use of TT (Trabecular Titanium) in hip arthroplasty surgery. Journal of Orthopaedic Traumatology 11, S53–S62.

Bertollo, N., et al., 2011. Effect of surgical fit on integration of cancellous bone and implant cortical bone shear strength for a porous titanium. Journal of Arthroplasty 26, 1000–1007.

Biemond, J., et al., 2011. Frictional and bone ingrowth properties of engineered surface topographies produced by electron beam technology. Archives of Orthopaedic and Trauma Surgery 131, 711–718.

Bobyn, J.D., et al., 1999. Characteristics of bone ingrowth and interface mechanics of a new porous tantalum biomaterial. Journal of Bone and Joint Surgery 81b, 907–914.

Bourne, R.B., et al., 2008. The next generation of acetabular shell design and bearing surfaces. Orthopedics 31 (Suppl. 2), 12.

Bragdon, C.R., et al., 1996. Differences in stiffness of the interface between a cementless porous implant and cancellous bone in vivo in dogs due to varying amounts of implant motion. Journal of Arthroplasty 11, 945–951.

Britton, J.R., et al., 2004. Measurement of the relative motion between an implant and bone under cyclic loading. Strain 40, 193–202.

Chang, J.-D., et al., 2011. Revision total hip arthroplasty using a tapered, press-fit cementless revision stem in elderly patients. Journal of Arthroplasty 26, 1045–1049.

Chanlalit, C., et al., 2011. Micromotion of plasma spray versus grit-blasted radial head prosthetic stem surfaces. Journal of Shoulder and Elbow Surgery 20, 717–722.

Cook, S.D., et al., 1991. Tissue growth into porous primary and revision femoral stems. Journal of Arthroplasty6 (Suppl.), S37S46.

Dayton, M.R., Incavo, S.J., 2005. Component loosening in total hip arthroplasty. Seminar on Arthroplasty 16, 161–170.

Engh, C.A., et al., 1992. Quantification of implant micromotion, strain shielding, and bone resorption with porous-coated anatomic medullary locking femoral prostheses. Clinical Orthopaedics and Related Research 285, 13–29.

Frenkel, S.R., et al., 2004. Bone response to a novel highly porous surface in a canine implantable chamber. Journal of Biomedical Materials Research B Applied Biomaterials 71, 387–391.

Gebert, A., et al., 2009. Influence of press-fit parameters on the primary stability of uncemented femoral resurfacing implants. Medical Engineering & Physics 31, 160–164.

Gilmour, L., et al., 2009. Mechanical properties of a sintered asymmetric particle ingrowth coating. In: ASM Materials and Processes Conference.

Gortz, W., et al., 2002. Spatial micromovements of uncemented femoral components after torsional loads. Transactions of the ASME 124, 706–713.

Gotze, C., et al., 2002. Primary stability in cementless femoral stems: custom-made versus conventional femoral prosthesis. Clinical Biomechanics 17, 267–273.

Kassi, J.P., et al., 2005. Stair climbing is more critical than walking in pre-clinical assessment of primary stability in cementless THA in vitro. Journal of Biomechanics 38, 1143–1154.

Kluge, W.H., 2009. Current developments in short stem femoral implants for hip replacement surgery. Orthopaedics and Trauma 23, 46–51.

Krischak, G.D., et al., 2003. Influence of preoperative mechanical bone quality and bone mineral density on aseptic loosening of total hip arthroplasty after seven years. Clinical Biomech 18, 916–923.

Levine, B.R., Fabi, D.W., 2010. Porous metals in orthopaedic applications—a review. Materialwissenschaft und Werkstofftech 41, 1002–1010.

Maher, S.A., et al., 2001. Measurement of the migration of a cemented hip prosthesis in an in vitro test. Clinical Biomechanics 16, 307–314.

Meneghini, R.M., et al., 2010. Bone remodeling around porous metal cementless acetabular components. Journal of Arthroplasty 25, 741–747.

Monti, L., et al., 1999. Methods for quantitative analysis of the primary stability in uncemented hip prostheses. Artificial Organs 23, 851–859.

Nogler, M., et al., 2004. Primary stability of a robodoc implanted anatomical stem versus manual implantation. Clinical Biomechanics 19, 123–129.

Ostbyhaug, P.O., et al., 2010. Primary stability of custom and anatomical uncemented femoral stems: a method for three-dimensional in vitro measurement of implant stability. Clinical Biomechanics 25, 318–324.

Park, Y., et al., 2010. The effect of abductor muscle and anterior-posterior hip contact load simulation on the in-vitro primary stability of a cementless hip stem. Journal of Orthopaedic Surgery 5 (40), 1–40.

Pilliar, R.M., et al., 1986. Observations on the effect of movement on bone ingrowth into porous-surfaced implants. Clinical Orthopaedics and Related Research 208, 108–113.

Race, A., et al., 2011. The addition of a hydroxyapatite coating changes the immediate postoperative stability of a plasma-sprayed femoral stem. Journal of Arthroplasty 26, 289–295.

Sakai, R., et al., 2006. Assessment of the fixation stiffness of some femoral stems of different designs. Clinical Biomechanics 21, 370–378.

Shirazi-Adl, A., et al., 1993. Experimental determination of friction characteristics at the trabecular bone/porous metal interface in cementless implants. Journal of Biomedical Materials Research 27, 167–175.

Soballe, K.S., et al., 1992. Tissue ingrowth into titanium and hydroxyapatite-coated implants during stable and unstable mechanical conditions. Journal of Orthopaedic Research 10, 285–299.

Valle, A.G., et al., 2004. Clinical and radiographic results associated with a modern, cementless modular cup design in total hip arthroplasty. Journal of Bone & Joint Surgery 86-A, 1998–2004.

Viceconti, M., et al., 2001. Even a thin layer of soft tissue may compromise the primary stability of cementless hip stems. Clinical Biomechanics 16, 765–775.

Westphal, F.M., et al., 2006. Migration and cyclic motion of a new short-stemmed hip prosthesis—a biomechanical in vitro study. Clinical Biomechanics 21, 834–840.

Zhang, Y., et al., 1999. Interfacial frictional behaviour: cancellous bone, cortical bone, and a novel porous tantalum biomaterial. Journal of Musculoskeletal Research 3, 245–251.